

## High- $T_c$ superconductivity in entirely end-bonded multi-walled carbon nanotubes

I.Takesue<sup>1,4</sup>, J.Haruyama<sup>1,4,\*</sup>, N.Kobayashi<sup>1</sup>, S.Chiashi<sup>2</sup>, S.Maruyama<sup>2</sup>, T.Sugai<sup>3,4</sup>, H.Shinohara<sup>3,4</sup>

<sup>1</sup>Aoyama Gakuin University, 5-10-1 Fuchinobe, Sagamihara, Kanagawa 229-8558 Japan

<sup>2</sup>Tokyo University, 7-3-1 Hongo, Bunkyo-ku, Tokyo 113-0033 Japan

<sup>3</sup>Nagoya University, Furo-cho, Chigusa, Nagoya 464-8602 Japan

<sup>4</sup>JST-CREST, 4-1-8 Hon-machi, Kawaguchi, Saitama 332-0012 Japan

\* Corresponding author; J-haru@ee.aoyama.ac.jp

**We report that entirely end-bonded multi-walled carbon nanotubes (MWNTs) can show superconductivity with the transition temperature  $T_c$  as high as 12K that is approximately 40-times larger than those reported in ropes of single-walled nanotubes. We find that emergence of this superconductivity is very sensitive to junction structures of Au electrode/MWNTs. This reveals that only MWNTs with optimal numbers of electrically activated shells, which is realized by the end-bonding, can allow the superconductivity due to intershell effects.**

One-dimensional (1D) systems face some obstructions that prevent the emergence of superconductivity, such as a Tomonaga-Luttinger liquid (TLL) [1][2], small density of states due to van-Hove singularity (VHS), and Peierls transition (charge-density waves). A carbon nanotube (CN), an ideal 1D molecular conductor, is one of the best candidates for investigating a possibility of 1D superconductivity and its correlation with such obstructions. Although a variety of intriguing quantum phenomena has been reported in CNs, only two groups have experimentally reported superconductivity (e.g., with a transition temperature ( $T_c$ ) as low as  $T_c = \sim 0.2\text{K}$  in ropes of single-walled CNs (SWNTs) [3] and that was identified only from the Meissner effect in arrays of very thin SWNTs [4]) to the best of our knowledge. In addition, those correlations with 1D phenomena as mentioned above have never been clarified.

In theoretical viewpoints, refs.[6]-[9] predicted that the correlation of TLL states with superconductivity is highly sensitive to phonon modes, electron-phonon coupling, strength of short-range attractive Coulomb interaction, and structures of ropes of CNs, allowing the appearance of superconductivity in specified cases. Ref. [24] also predicted importance of electron-phonon interaction for superconductivity in very thin CNs. However, these have not yet been experimentally verified. To the best of our knowledge, confirmed reports of superconductivity in 1D conductors are only in organic materials [10].

Here, in refs. [11] - [13], we have successfully realized end-bonding of multi-walled CNs (MWNTs) synthesized in nanopores of alumina templates. Recently, we also realized proximity-induced superconductivity (PIS) by end-bonding MWNTs, which were prepared using the same method, in Nb/MWNTs/Al junctions [11][12]. They proved that the Cooper pairs could be effectively transported without destruction only through the highly transparent interface of the CNs/Nb junctions obtained by this end-bonding. Such an entire end-bonding has never been carried out in conventional field-effect transistor (FET) structures using CNs as the channels. .

Following the method with nano-porous alumina templates but employing some specified conditions [14] (Fe/Co catalyst and Methanol gas), we synthesized arrays of Au/MWNTs/Al junctions (Fig.1(a)) and investigated a possibility of superconductivity in MWNTs in this study. Figure 1(d) shows a plane transmission electron microscope (TEM) image of the array shown in (a). MWNTs are clearly visible in many pores. In the inset, a high-resolution cross-sectional TEM image of a MWNT is shown. Structures of this MWNT are similar to those in conventional MWNTs. It also includes no Fe/Co catalyst, which tends to destroy Cooper pairs, in the entire region. Figure 1(e) shows a result of resonance Raman measurements of the MWNTs. Only a large peak is observed significantly around  $1600\text{ cm}^{-1}$  (the so-called G-band). This strongly indicates that the MWNTs have high quality without defects. Absence of ferromagnetic catalyst and defects in the MWNTs with high quality are very different from those in our previous studies [11]-[13].

We prepared three-different types of Au electrode/MWNTs junctions using this MWNT as shown

in Fig.1 [15] in order to investigate importance of end-bonding and intershell effects for realization of superconductivity; i.e., **(1)** Entire Au-end junctions (Fig.1(a)), **(2)** Partial Au-end junctions (Fig.1(b)), and **(3)** Au-bulk junctions (Fig.1(c)). For (1) realized by sufficient cutting of MWNTs accumulated on the template surface [15], it was already proven that this method could allow making contact of Au electrode to the entire circumference of a top end of shell and making such a contact to all the shells of a MWNT in refs. [11]-[13] (red lines in Fig.1(a)), resulting in the entire end-bonding. In contrast, for (2) obtained from insufficient cutting, only partial shells could have end-contacts to Au (Fig.1(b)). For (3) obtained from no cutting, only the outermost shell could have contact to the Au electrode as reported in previous studies [5][19] (Fig.1(c)). Each structure was confirmed by high-resolution cross-sectional TEM observations.

Figure 2 shows electrical properties in the entire Au-end junction sample. Fig.2(a) shows the zero-bias resistance ( $R_0$ ) as a function of temperature.  $R_0$  increases with decreasing temperatures and one can confirm an apparent superconducting transition with the onset  $T_c$  as high as 12K and the temperature ( $T_c(R = 0)$ ), at where the  $R_0$  drops to 0  $\Omega$ , as high as  $T = 7.8K$ . These values for onset  $T_c$  and  $T_c(R = 0)$  are at least approximately 25- and 40-times, respectively, higher than those reported in SWNT ropes [3].

Figure 2(b) shows the differential resistance as a function of current for different temperatures. A low and broad resistance peak exists at  $T = 12K$ . This peak disappears suddenly and a resistance dip appears  $T = 11.5K$ . The depth and width of this resistance dip monotonically increase as the temperature decreases, corresponding to the abrupt  $R_0$  drop in Fig.2(a), and attain at zero  $\Omega$  at  $T = \sim 8K$ . The value of superconducting gap  $\Delta \approx 1.15$  meV observed at  $T = 8K$  in this sample is in excellent agreement with the Bardeen-Cooper-Schrieffer (BCS) relation  $\Delta = 1.76kT_c$ , when  $T_c(R=0) = 7.8K$  is employed. Moreover, the behaviors of critical current ( $I_c$ ) in normalized temperatures as shown in the inset is also in excellent agreement with the Ginzburg-Landau (GL) critical current behavior for a homogeneous order parameter,  $I_c \propto [1 - (T/T_c)^2]^{3/2}$  [17]. These agreements support that the abrupt  $R_0$  drop confirmed in Fig.2(a) and the corresponding resistance dip in Fig.2(b) are indeed attributed to superconductivity, which is strongly associated with that of the BCS type.

Figure 2(c) shows the differential resistance as a function of current for different magnetic field ( $H$ ). The resistance dip is actually destroyed by applied fields like conventional superconducting behaviors as shown in the main panel of Fig.2(c). The drastic increase of  $R_0$  from zero fields with a field increase (inset) differs greatly from that in SWNT ropes [4]. This low critical field implies that the observed superconductivity is either type-I or type-II without defects for pinning of the magnetic fluxes penetrating the MWNTs. Alternatively, this may indicate the presence of strong electron-acoustic phonon coupling, as reported by Ando et al. [18], since a huge magnetoresistance was predicted to have appeared even under small magnetic fields in CNs with strong electron-acoustic phonon coupling. Such coupling can cause superconductivity with high  $T_c$ .

Consequently, we have confirmed that the entirely end-bonded MWNTs could show superconductivity with  $T_c$  as high as 12K from **1**. An abrupt  $R_0$  drop down to  $0 \Omega$ , **2**. Agreement of the observed resistance dip and superconducting gap  $\Delta$  following BCS relation  $\Delta = 1.76kT_c$ , **3**. Critical current behavior qualitatively following  $I_c \propto [1 - (T/T_c)^2]^{3/2}$ , and **4**. Destruction of the observed resistance dip by applied magnetic field. We have also confirmed that six samples have exhibited such high- $T_c$  features (i.e., onset  $T_c = 6 \sim 12$ K) to date. In addition, we have found that some of these samples have indeed exhibited diamagnetism (i.e., Meissner-effect like behaviors) in SQUID measurements to date. Because, however, it cannot yet be exactly identified as Meissner effect from some reasons at current stage, further investigation is required. In this viewpoint, this study is analogous to ref.[3], which reported superconductivity with  $T_c = 0.2$ K only from resistance drops but did not show Meissner effect.

Here, we show electrical properties in the Au-bulk junction sample in Fig.3 and the partial Au-end junction sample in Fig.4. As shown in Fig.3, no  $R_0$  drop was observable in measured entire temperatures in the Au-bulk junction sample.

As shown in the main panel of Fig.4(a), in the partially end-bonded sample,  $R_0$  increases with decreasing temperatures and gradually saturates. Then, only a small  $R_0$  drop (i.e., a sign of superconductivity) appeared below  $T = \sim 3.5$ K without a  $R_0$  decrease down to  $0 \Omega$  at  $T = 1.5$ K (inset of Fig.4(a)). Most of samples have shown this sign of superconductivity to date.

The behaviors of the differential resistance as a function of current for different temperatures shown in Fig.4(b) differs greatly from that observed in Fig.2(b), since it includes the temperature dependence of the resistance peak as follows. A large and broad resistance peak is observable at  $T = 4.5$ K. It grows and broadens as the temperature decreases, corresponding to  $R_0$  increase in Fig.4(a), and mostly disappears at  $T = 2.5$ K. In contrast, a resistance dip with a narrow width begins to be observed at the center of this peak at  $T = 4$  K and the depth monotonically deepens in a temperature decrease. A corresponding small  $R_0$  drop can appear only below  $T = 3.5$  K (Fig. 4(a)), resulting from the superposition of growth of the resistance peak and deepening of the resistance dip at zero current. Importantly, presence of this large resistance peak prevents both the emergence of resistance dip at  $T \geq 4.5$  K and the  $R_0$  drop at  $T \geq 3.5$ K, unlike Fig.2. The residual resistance is still large even at  $T = 1.5$  K due to this resistance peak

Figure 4(c) exhibits a qualitatively similar destruction of the resistance dip and an increase in  $R_0$  to those in Fig.2(c).

Here, we discuss origins for the observed differences in superconductivity, which strongly depend on the junction structures of Au/MWNTs. One of the origins is the effective transport of Cooper pairs from the MWNTs to the Au electrode via the highly transparent interface, which was realized only in the entire Au-end junctions, as proven in refs. [11] - [13].

Moreover, power law behaviors in relationships of  $G_0$  versus temperatures (i.e.,  $G_0 \propto T^\alpha$ ;

monotonic  $R_0$  increase with decreasing temperatures) and those correlations with emergence of superconductivity, which strongly depend on junction structures, were confirmed at temperatures  $> T_c$  for Figs.2(a), 3, and 4(a). These stress possible presence of competition between superconductivity and TLL states as one of the origins for the observed junction dependence.

TLL states, which are a non Fermi-liquid state arising from an 1D repulsive electron-electron interaction, have been frequently reported by observing power laws (i.e.,  $G_0 \propto E^\alpha$ , where  $E$  is the energy) in both MWNTs [1][5] and SWNTs [2]. Recently, its correlation with superconductivity has attracted much attention as mentioned in introduction [11] - [13]. The values of  $\alpha$  mean the strength of an electron-electron interaction and were extremely sensitive to the junction structures of electrodes/CNs. Ref. [1] reported  $\alpha_{\text{bulk}} = \sim 0.3$  for Au-bulk junction and  $\alpha_{\text{end}} = \sim 0.7$  for Au-end junction [22]. We found that  $\alpha = \sim 0.7$ ,  $\sim 0.8$ , and  $\sim 0.3$  estimated from the power laws at  $T > T_c$  for Figs.2 (a), 4(a) and 3, respectively, are in good agreement with these  $\alpha_{\text{end}}$  and  $\alpha_{\text{bulk}}$ . This result proves the actual presence of Au-end and Au-bulk junctions in our systems as well as the presence of TLLs in these MWNTs.

Only the  $G_0 \propto T^{-0.3}$  relationship was confirmed in all the temperatures in the Au-bulk junction sample. This is consistent with refs. [5] and [20], which reported that only the (second) outermost shell became electrical active in the Au-bulk junction of MWNT-FETs and that exhibited TLLs in MWNTs. This is why most of MWNT-FETs with electrode-bulk junctions in previous reports have not exhibited superconductivity. This result means that a SWNT with a large diameter cannot take a superconducting transition because superconductivity cannot overcome TLL states [6].

In contrast, the  $G_0 \propto T^{-0.7}$  relationship at  $T > T_c$  abruptly disappeared and the superconductive phase emerged at  $T_c=12\text{K}$  with decreasing temperatures in the entire Au-end junction sample, whereas the  $G_0 \propto T^{-0.8}$  relationship gradually saturated and a sign of superconductivity appeared around  $T = 3.5\text{ K}$  in the partial Au-end junction sample. The former stresses that superconductivity can easily overcome the TLL states, while the latter means that superconductivity competes with the TLL states. In Figs.2(b) and 4(b), these behaviors in TLL states and superconducting transition correspond to the competition of the resistance peak and the resistance dip, respectively.

Here, the entire end-bonding of MWNTs could make all the shells to be electrically active, while only partial numbers of shells were electrically active in the partial Au-end junctions. These indicate that the competition between TLLs and superconductivity mentioned above are at least strongly associated with the number of electrical active shells ( $N$ ) of the MWNTs (i.e.,  $N = 1$  for Fig.3,  $N = 9$  for Fig.2(a), and  $1 < N < 9$  for Fig.4(a)). This stresses that intershell effects of the MWNTs play the key role for the emergence of high- $T_c$  superconductivity, which overcomes the TLL states.

In fact, the intershell effects in MWNTs have been discussed for the TLLs predicting that the TLL was sensitive to the values of  $N$  of the MWNT [1][19] and that this theory was applicable also to SWNT ropes. Moreover, indeed, the importance of the intertube effects for the appearance of

superconductivity competing with TLLs has been predicted in ropes of SWNTs [7] as follows.

The TLLs were suppressed by intertube charge coupling (i.e., coupled TLLs; sliding TLLs [16]), because the intertube electron hopping (tunneling) was prohibited due to misalignment of carbon atoms between SWNTs with different chiralities and diameters. In contrast, the intertube Cooper-pair hopping was allowed and, hence, an intratube short-range attractive Coulomb interaction grew over the SWNTs in a temperature decrease. Both effects and, hence,  $T_c$  were enhanced as the number of SWNTs in a rope and the strength of intratube short-range attractive Coulomb interaction increased.

One can qualitatively interpret our results mentioned above by replacing SWNTs in a rope in this model [7] to shells in a MWNT (i.e., replacing intertube effects to intershell effects). Because the differences in chiralities and diameters among shells in a MWNT are greater than those among SWNTs in a rope, this model will bring more significant results in MWNTs. For a quantitative interpretation of these intershell effects, experimental clarification of the dependence of  $T_c$  on  $N$ ,  $\alpha$ , and strength of intrashell attractive Coulomb interaction is also crucial.

Moreover, the following points are interesting and should be revealed; **1.**It is indispensable to get higher reproducibility for the entire end-bonding in order to obtain higher reproducibility of high- $T_c$  samples, **2.** Confirmation of Meissner effect, **3.** Enhancement of  $T_c$  by carrier doping, **4.** Influence of curvature (i.e., tube structure and small diameter) in MWNTs on  $\pi - \sigma$  orbital coupling and electron-phonon interaction, and those correlations with  $T_c$  [24] in comparison with 2D-layered superconductors (e.g.,  $MgB_2$ , high- $T_c$  oxide superconductors, and graphite-related superconductors), **5.** Correlation of VHS with  $T_c$ , because VHSs in each single shell are superposed in a MWNT, resulting in a peak-width broadening in VHS and an increase in density of states around Fermi levels, and **6.** Influence of coupling of neighboring MWNTs in an array, because this might screen electron-electron interaction. Finally, application of these superconducting MWNTs to molecular quantum computation is also strongly expected [23]. A MWNT can be strongly expected to be a molecular conductor promising for 1D superconductivity.

We greatly thank J.Akimitsu, R.Saito, S.Saito, S.Tarucha, Y.Iye, W.Tsukada, J.-P. Leburton, M.Dresselhaus, and D.Loss for fruitful discussions and encouragement. We also thank N.Sugiyama for the nice plane TEM image and J.Mizubayashi for the help in Raman spectrum measurements.

## References

1. A.Bachtold, C.Shonenberger, et al., Phys.Rev.Lett. 87, 166801 (2001)
2. M.Bockrath, et al., Nature 397, 598 (1999); H.Ishii, H.Kataura, et al., Nature 426, 540 (2003)
3. M. Kociak, H. Bouchiat, et al., Phys. Rev. Lett. 86, 2416 (2001)
4. Z. K. Tang, et al., Science 292, 2462 (2001)
5. A.Bachtold, et al., Nature 397, 673 (1999); M.R.Buitelaar, et al., Phys.Rev. Lett. 88, 156801 (2002)
6. D.Loss and T.Martin, Phys. Rev. B 50, 12160 (1994-II)
7. J.Gonzalez, Phys.Rev.Lett. 88, 076403 (2002); A.Sedeki, et al., Phys.Rev.B 65, 140515(R) (2002); J.Gonzalez, Phys.Rev.Lett. 87, 136401 (2001)
8. De Martino and R.Egger, Phys.Rev.B 67, 235418 (2003)
9. J.Gonzalez, et al., Phys.Rev. B 63, 134421 (2001)
10. I.J.Lee, et al., Phys. Rev. Lett. 78, 3555 (1997)
11. J.Haruyama, et al., Phys.Rev.B 68, 165420 (2003); Appl.Phys.Lett. 84, 4714 (2004); Microelectronics Journal 34, 537 (2003); Physica C 408, 85 (2004)
12. J.Haruyama, et al., Phys.Rev.Lett. In submission; Physica Stat. Sol. (b) 242(2), 265 (2005)
13. J. Haruyama, et al., Phys. Rev. B 65, 33402 (2002); Pys.Rev.B, 073406 (2001)
14. S. Maruyama, et al., Chem. Phys. Lett. 360, 229 (2002).
15. Electrochemical deposition time of Fe/Co catalyst into the bottom of the pores and time of ultrasonic cleaning for cutting the MWNTs [11], which grew above the pores and accumulated on the template surface, before evaporating Au electrode were optimized for each structure.
16. A.Vishwanath and D.Carpentier, Phys.Rev.Lett. 86, 676 (2001)
17. M.Tinkam, *Introduction to Superconductivity* (McGraw-Hill, New York 1996)
18. H.Suzuura and T.Ando, Phys.Rev.B 65, 235412 (2002)
19. R.Egger, Phys.Rev.Lett. 83, 5547 (1999)
20. M.R.Buitelaar, C.Shonenberger, Phys.Rev. Lett. 89, 256801 (2002)
21. I.Takesue, T.Akazaki. J.Haruyama., H.Takayanagi, et al., Physica E 24, 32 (2004); P.Recher and D. Loss, Phys. Rev. B 65, 165327 (2002); C.Bena et al., Phys.Rev.Lett.89, 037901 (2002)
22. This interpretation for the origin of power laws is still on debating stage. A Coulomb blockade strongly coupled with its external electromagnetic environment and a phenomenon related to 1D localization may explain them.
23. From this viewpoint, ref. [21] indicated that the TLLs of CNs tend to separate Cooper pairs into individual spins in PIS state. If Cooper pairs in CNs actually have a strong entanglement [12][20], even such separated spins can retain a strongly entangled state. This results in molecular spin-entanglers.
24. R.Barnett, E.Demler, and E.Kaxiras, Phys.Rev.B 71, 035429 (2005)

## Figure captions

**Figure 1:** Schematic cross-sections of Au/MWNTs interfaces in Au/MWNTs/Al junctions prepared in nano-pores of alumina templates for **(a) Entire Au-end** **(b) Partial Au-end** and **(c) Au-bulk** junctions. Each one nano-pore includes one MWNT. Solid lines in a MWNT are the shells and red lines are the shells where can have electrical contacts to Au electrodes, in each MWNT. The lengths of MWNTs are  $\sim 0.6 \mu\text{m}$ . Quasi-four terminal measurements were performed by attaching lead lines to Au electrode and Al substrate. Approximately  $10^3 \sim 10^4$  MWNTs exist under an electrode.

**(d)** Plane TEM image of the MWNT array, which were shown in Fig.1(a) and used for Figs.2(a), 3(a), and 4(a). This image was observed around the top end of an alumina template. MWNTs were shown by arrows. **Inset:** High-resolution cross-sectional TEM image of a typical MWNT. The MWNT has a diameter of  $\sim 7.4 \text{ nm}$ , the number of shells of 9, the shell thickness of  $\sim 2.7 \text{ nm}$ , and the intershell spacing of  $\sim 3.4 \text{ \AA}$ .

**(e):** A result of resonance Raman measurements of the MWNT by laser energy of 2.41 eV.

**Figure 2:** Electrical properties in the entire Au-end junction sample. The residual resistance  $< \sim 0.5 \text{ ohm}$  has been subtracted in the figures.

- (a)** Zero-bias resistance ( $R_0$ ) as a function of temperatures at zero-magnetic field ( $H = 0 \text{ T}$ ).
- (b)** Differential resistance as a function of current at  $H = 0 \text{ T}$  for different temperatures. The numbers noted on each curve denote the temperatures in Kelvin. Resistance oscillations similar to those in refs. [3][11] (interpreted as a phase slip) are observable in the large current regions at  $T \leq 8.5 \text{ K}$ . **Inset:** Relationship of critical current ( $I_c$ ) vs temperature normalized for comparison with the Ginzburg-Landau critical current behavior. The solid line is provided just to the eyes.
- (c)** Differential resistance as a function of current at  $T = 1.5 \text{ K}$  for different magnetic fields. The number noted on each curve is the magnetic field in Tesla, which was applied perpendicular to the tube axis. **Inset:**  $R_0$  as a function of magnetic field.

**Fig. 3:**  $R_0$  as a function of temperatures for the Au-bulk junction sample.

**Fig. 4:** Electrical properties in the partial Au-end junction sample.

- (a)  $R_0$  as a function of temperatures. **Inset :** Expansion of the main panel for  $1.5 \text{ K} \leq T \leq 5 \text{ K}$ .
- (b) Differential resistance as a function of current for different temperatures.
- (c) Differential resistance as a function of current for different magnetic fields. **Inset:**  $R_0$  as a function of magnetic field.

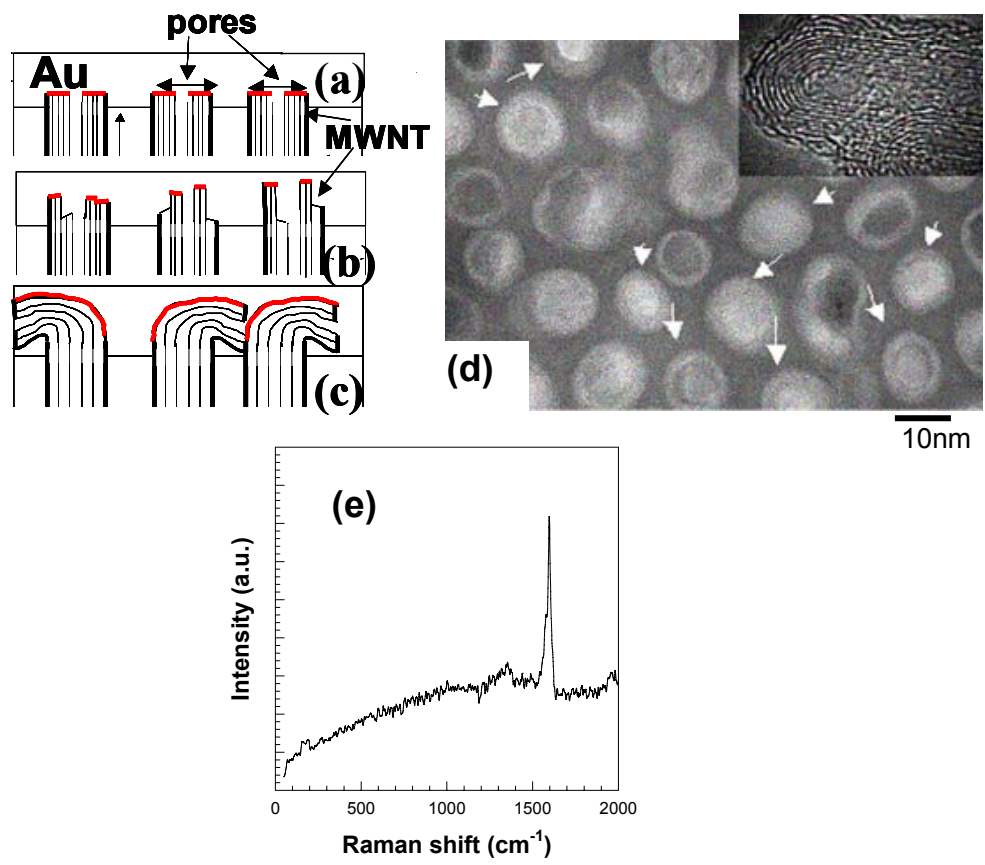


**Fig.1**

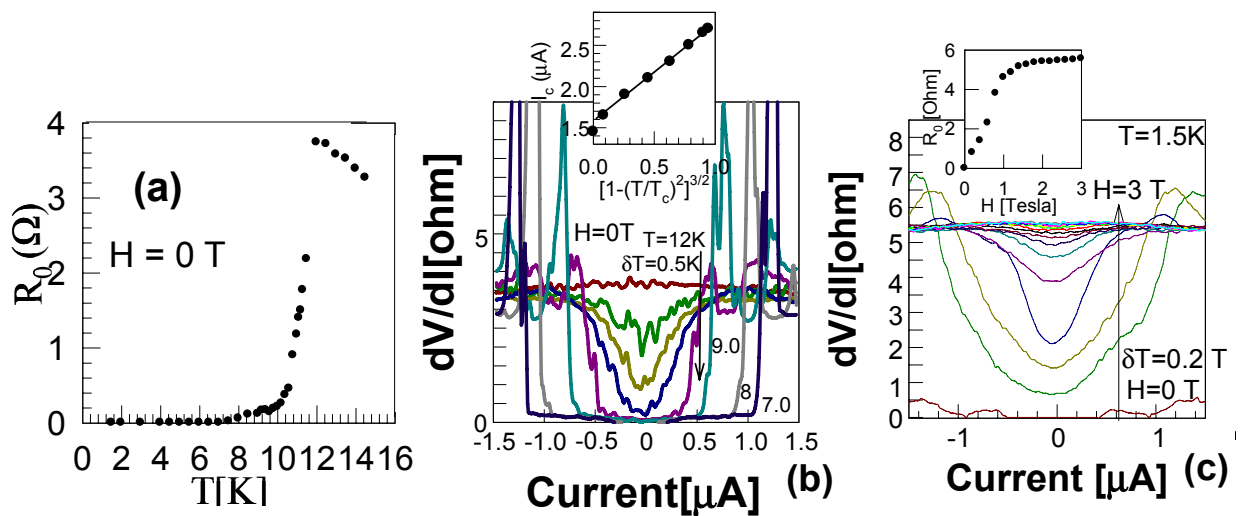


Fig.2

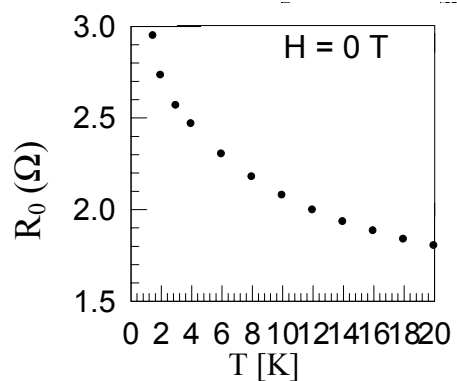


Fig.3

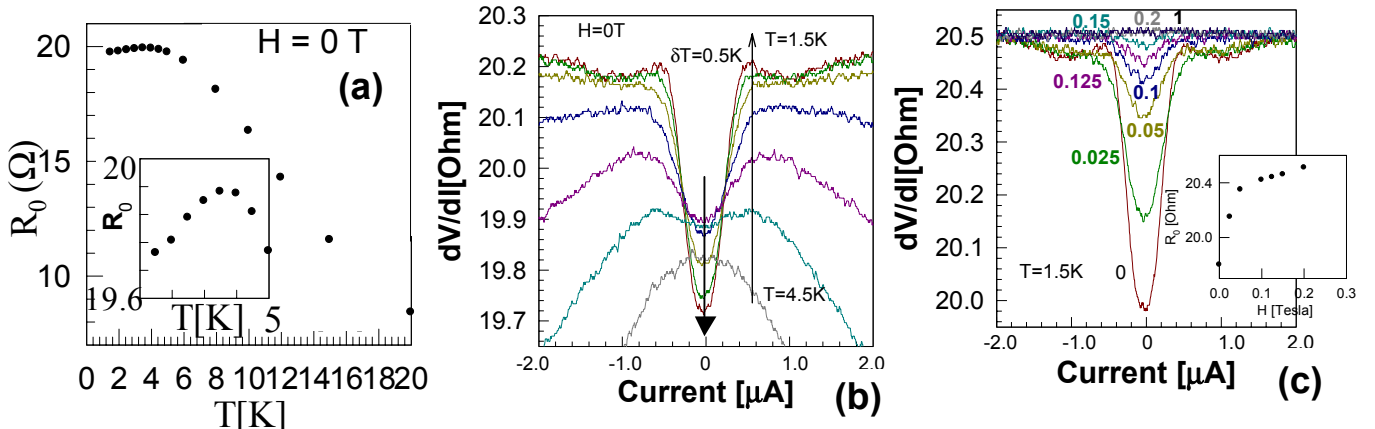


Fig.4